Correlating Wettability, Adhesion, and Friction on Micro/Nano-Engineered Hydrophobic Surfaces

1.Bathi Prasad, 2.B.H.Nagesh, 3.Hemanth Kumar

Department of Marine Engineering,
Andhra University,
Visakhapatnam , AP, INDIA.

ABSTRACT:

This study presents the fabrication of hydrophobic MNESs exhibiting superior adhesion and friction properties. The process involves a combination of aluminum-induced crystallization (AIC) of amorphous silicon (a-Si) and octadecyltrichlorosilane (OTS) coating. AIC was employed to create micro/nano-textured silicon surfaces, while subsequent OTS self-assembled monolayer (SAM) formation reduced surface energy.

Wetting behavior was characterized using a video-based contact angle measurement system, revealing the hydrophobic nature of the MNESs. Adhesion and friction properties were evaluated with a TriboIndenter. Results demonstrate a significant enhancement in both adhesion and friction performance of all MNESs compared to untreated silicon substrates. Moreover, a strong correlation was observed between the adhesion/friction properties of OTS-modified textured surfaces and their hydrophobicity, as quantified by water contact angle measurements. Higher contact angles corresponded to improved adhesion and friction performance.

INTRODUCTION:

Adhesion and friction forces pose significant challenges in micro-electro-mechanical systems (MEMS) due to the devices' inherently large surface area-to-volume ratios and extremely small inter-component gaps[1,2].

Mitigation strategies for adhesion and friction in MEMS involve either topographical modification through surface texturing or compositional alteration by applying low surface energy coatings[1,2].

Surface texturing effectively reduces adhesion and friction by decreasing the contact area between surfaces. Simultaneously, enhancing surface hydrophobicity through low surface energy materials diminishes capillary forces, thereby mitigating adhesion and friction. This study focuses on creating superhydrophobic/hydrophobic surfaces to investigate their wetting, adhesion, and friction characteristics.

Water contact angle (WCA) is a critical metric for quantifying surface hydrophobicity. Surfaces with WCAs below 90° are hydrophilic, while those exceeding 90° are hydrophobic. Super hydrophobicity is characterized by WCAs greater than 150°. While chemical modification can render smooth silicon surfaces hydrophobic with WCAs up to 120°, achieving super hydrophobicity necessitates additional surface texturing [3].

To attain superhydrophobicity, surface texturing is indispensable. The Cassie-Baxter model elucidates the influence of topography on water contact angle (WCA) [4]. This model posits that a water droplet rests on a rough surface, entrapping air within the surface asperities[5–7]. The apparent contact angle, θ, is described by:

$\cos \theta = f_1$

$\cos \theta - f_2$

where θ is the WCA of a smooth surface with identical chemistry, f_1 is the solid-liquid interfacial area fraction, and f_2 is the air-liquid interfacial area fraction. By judiciously combining surface texturing and chemical modification, it is feasible to engineer surfaces exhibiting a θ significantly surpassing that of the corresponding smooth surface. $f_1 + f_2 = 1$.

Numerous techniques have been reported for creating superhydrophobic surfaces[10], including those employing nanofibers, carbon nanotubes[8], nanorods [9], plasma etching[11], and electrochemical deposition[12]. While these methods offer varying advantages, many are incompatible with MEMS fabrication processes, complex to implement on MEMS structures, or suffer from other limitations.

This study presents a MEMS-compatible approach for generating superhydrophobic surfaces to mitigate adhesion and friction. The method involves creating silicon micro/nano-textured surfaces (MNTSs) through aluminum-induced crystallization (AIC) of amorphous silicon (a-Si), followed by the application of octadecyltrichlorosilane (OTS) self-assembled monolayers (SAMs) to reduce surface energy.

OTS self-assembled monolayers (SAMs) have been extensively investigated to enhance the tribological performance of smooth surfaces[13–15]. Aluminum-induced crystallization (AIC) of amorphous silicon (a-Si) has been employed to produce large-grained polycrystalline silicon films for electronic and photovoltaic applications[16–21]. However, the utilization of AIC for generating micro/nano-textured surfaces (MNTSs) for tribological purposes is novel. This research integrates AIC of a-Si and OTS SAM formation to produce superhydrophobic/hydrophobic surfaces aimed at reducing surface adhesion and friction forces.

2.EXPERIMENTAL DETAILS:

2.1. Fabrication of textured surfaces by AIC of a-Si:

Silicon (100) wafers with a polished single side served as substrates for fabricating MNTSs via AIC of a-Si. A standard cleaning process involving acetone, isopropanol, and deionized (DI) water was followed by a wet oxidation at 950 °C for 8 hours to grow a ~2 µm thick silicon dioxide layer. This oxide layer acted as a buffer, preventing substrate crystal orientation from influencing the a-Si crystallization process.Amorphous silicon films with thicknesses ranging from 100 nm to 400 nm were deposited onto the oxidized wafers using plasma-enhanced chemical vapor deposition (PECVD). PECVD parameters, including RF power (20 W), chamber pressure (133 Pa), substrate temperature (250 °C), and SiH4 flow rate (85 sccm), were maintained constant. Following deposition, samples were exposed to ambient air for three days to form a uniform native oxide layer on the a-Si surface. Finally, an 800 nm thick aluminum layer was thermally evaporated onto the prepared samples.

The samples were diced into 1 x 1 inch squares and subjected to air annealing in a conventional furnace at temperatures ranging from 750 °C to 850 °C for durations of 5 to 20 seconds. Subsequent air cooling was performed. The excess aluminum was removed through wet selective etching using "Aluminum Etchant - Type D" (Transene Company, Inc.) at 50 °C for approximately 15 minutes. This etching process revealed the underlying silicon micro/nano-structures, forming the desired silicon MNTSs[22]. It is crucial to note that the process parameters employed in this study deviate significantly from those typically used in traditional a-Si AIC, as detailed in our previous work[16–21].

2.2. OTS SAM deposition:

Both MNTSs and thermally oxidized smooth silicon control samples underwent a piranha solution (3:7 H_2O_2:H_2SO_4) cleaning process at room temperature for an hour. This step removed surface contaminants and introduced a fresh oxide layer to enhance OTS adhesion. Subsequent rinsing with DI water and toluene, followed by N_2 drying, prepared the samples for OTS deposition.

The samples were immersed in a 1% (mass concentration) OTS/toluene solution for 10 minutes to facilitate uniform OTS self-assembly. A final cleaning process involving chloroform rinsing and ultrasonic bath cleaning in chloroform ensured removal of residual solvents, with subsequent air drying completing the process. These OTS deposition parameters were optimized based on previous studies[23].

2.3. Sample characterization:

2.3.1. Topography characterization:

Scanning electron microscopy (SEM) was employed to characterize the surface topography of both oxidized smooth silicon samples and MNTSs produced via a-Si AIC, both before and after OTS deposition. SEM micrographs were captured at various magnifications and locations using an FEI XL30 environmental SEM operating at 10 kV to assess the micro-scale uniformity of the micro/nano-textures.

Top-down, oblique-angle, and cross-sectional views were acquired. Top-down images provided information on the lateral dimensions, areal coverage, and density of micro/nano-textures. Oblique-angle views revealed the texture shape, while cross-sectional images enabled estimation of micro/nano-structure heights. ImageJ software was used to extract average texture size, count, and areal coverage (area fraction) from the micrographs.

2.3.2. Wettability characterization:

A video-based contact angle measurement system was employed to quantify the water contact angles (WCAs) of the samples. Static WCAs were determined by the sessile drop method, involving the deposition of five 7 µL DI water droplets on each sample surface. Sliding angles were measured by placing a water droplet on a superhydrophobic sample mounted on a tilting stage. The stage inclination was adjusted incrementally (0.03° resolution) until droplet sliding occurred. All WCA measurements were conducted under ambient laboratory conditions (approximately 20 °C, 45% relative humidity).

2.3.3. Adhesion and friction tests:

Adhesion (pull-off) and friction tests were performed under ambient conditions (approximately 45% relative humidity) using a TriboIndenter equipped with force and displacement sensing capabilities in both vertical and lateral directions. The instrument employed capacitive force-displacement transducers with electrostatic actuation and measured displacements using a differential capacitor technique. The system exhibited a vertical displacement resolution of 0.02 nm (0.2 nm noise floor), vertical/indentation force resolution of 3 nN (100 nN noise floor), and lateral force resolution of 500 nN (5 µN noise floor).

Adhesion tests on textured samples involved a 100 µm radius diamond conical tip following a predefined displacement profile: approach from 50 nm, indentation (1-80 nm), and withdrawal. The adhesion force was determined as the maximum force required to separate the tip from the sample during withdrawal. However, the strong adhesion of the 100 µm tip to smooth silicon surfaces prevented meaningful adhesion measurements due to instrument overload.

To address this, adhesion tests on smooth samples were conducted using a 5 µm radius tip. Previous studies have demonstrated a linear relationship between adhesion force and SPM tip radius. By applying a tip radius correction factor, the results obtained with the 5 µm tip could be compared to those expected for a 100 µm tip.

Friction performance was evaluated using a diamond tip with a 100 µm radius of curvature. A contact force of 2 µN was initially applied to the sample surface, followed by the application of normal loads ranging from 250 µN to 1500 µN. The tip was then moved across the surface at a constant speed of 1 µm/s. Normal and lateral displacements, as well as corresponding forces, were recorded continuously during sliding[24]. The coefficient of friction (COF) was calculated as the average ratio of lateral to normal force during sliding. Friction tests were conducted at multiple locations on each sample to ensure data reliability.

3. Results and discussion

3.1. Topographies of MNTSs:

Figure 1 presents representative SEM micrographs of an oxidized silicon wafer and a micro/nano-textured sample. Figure 1(a) depicts a smooth oxidized silicon wafer surface at a magnification of 5000x. In contrast, Figure 1(b) showcases a nano-textured surface obtained after the a-Si AIC process, also at a magnification of 5000x. The latter reveals irregularly shaped micro- and nanoscale islands of varying sizes.

A higher magnification (20,000x) oblique-angle SEM image (Figure 1(c)) provides further details about the textures. These irregularly shaped features are randomly distributed across the surface, with lateral dimensions and heights ranging from tens to hundreds of nanometers. Energy dispersive spectroscopy, X-ray diffraction, and electron diffraction analyses confirmed that these structures are crystalline silicon grains with a (111) orientation, excluding the possibility of residual aluminum[22].

SEM analysis of both smooth silicon surfaces and MNTSs after OTS SAM deposition did not reveal any aggregated OTS islands or discernible changes in surface topography. This indicates that the OTS self-assembly process did not alter the morphology of either the smooth or textured surfaces.

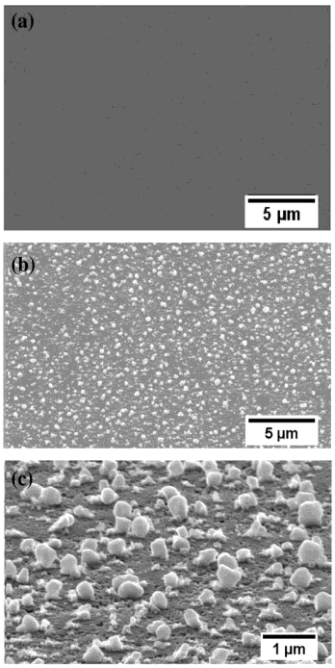

Fig. 1. SEM micrographs of (a) a smooth oxidized silicon surface (top down view),(b)a nano-textured surface (top down view), and

(c) the nano-textures on the surface (70° oblique-angle view).

3.2. Surface wetting properties:

The wetting properties of oxidized smooth silicon surfaces and MNTSs (Figure 1(a) and 1(b)), both before and after OTS deposition, were assessed using a video-based contact angle measurement system. As shown in Figure 2(a) and 2(b), the WCA of the oxidized smooth silicon sample increased from 46° to 112° following OTS SAM deposition. This 112° WCA aligns with reported values for OTS-coated smooth silicon surfaces[25], indicating complete OTS coverage. Figure 2(c) and 2(d) present the WCAs of the textured sample, which increased from 37° to 155° after OTS deposition. Additionally, the sliding angle of OTS-modified MNTSs was measured to be less than 1°.

The significantly higher WCA of the OTS-modified textured surface (155°) compared to the OTS-modified smooth surface (112°) underscores the crucial role of surface texturing in enhancing hydrophobicity. The

superhydrophobicity of the OTS-modified textured silicon surfaces can be attributed to a combination of chemical and topographical factors. Prior to OTS deposition, the oxidized silicon surface exhibited hydrophilic behavior due to the presence of terminal oxygen atoms. Subsequent OTS self-assembly replaced these hydrophilic groups with hydrophobic alkyl chains, rendering the surface hydrophobic. The introduction of surface texture further amplified hydrophobicity by trapping air between the water droplet and the textured surface, minimizing droplet-solid contact area.

3.3. Adhesion and friction properties:

Figure 3(a) presents a comparative analysis of adhesion force (logarithmic scale) versus indentation displacement for smooth and textured samples, both before and after OTS modification. Despite employing a significantly smaller radius tip (5 µm) for the smooth silicon sample, its adhesion force remains substantially higher than those of the other three samples (nano-textured, OTS-modified smooth, and OTS-modified nano-textured) tested with a 100 µm tip. This observation clearly demonstrates that both surface texturing and OTS modification effectively reduce adhesion forces.

The reduction in adhesion forces for textured and OTS-modified smooth surfaces can be attributed to the following: previous studies have established a near-linear relationship between adhesion force and SPM tip radius[24].

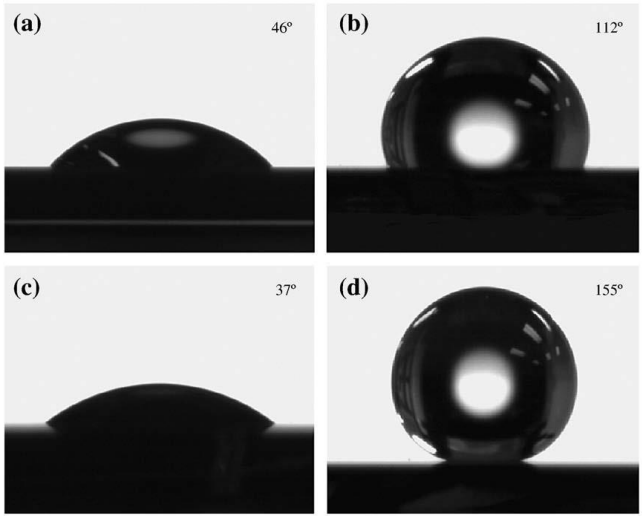

Fig. 2. WCA pictures of (a) a smooth oxidized silicon surface before the OTS deposition, (b) the smooth surface after the OTS deposition, (c) a nano-textured before the OTS deposition, and (d) the textured surface after the OTS deposition.

Contact area significantly influences adhesion forces. On a smooth surface, the contact area between the diamond tip and the sample is primarily determined by the tip's radius of curvature. However, for textured surfaces, the contact area is restricted by the dimensions of the micro/nano-islands, which are substantially smaller than the tip radius. Consequently, textured surfaces exhibit significantly reduced real contact areas compared to smooth surfaces, leading to lower adhesion forces.

The hydrophobic nature of OTS SAMs further contributes to reduced adhesion by minimizing water adsorption and subsequent meniscus formation. While both surface texturing and OTS modification decrease adhesion, texturing appears to be more effective due to increased surface separation and reduced likelihood of meniscus formation. The combination of texturing and OTS modification on a single surface yields the lowest adhesion among all samples tested.

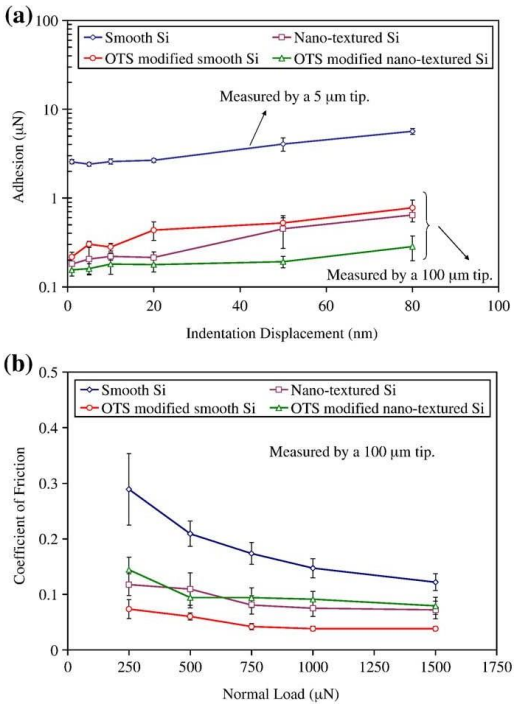

Fig. 3. Comparisons of (a) adhesion and (b) friction properties of a smooth and a nano- textured sample before and after OTS SAM modifications.

Figure 3(b) illustrates the relationship between coefficient of friction (COF) and normal load for the four samples. Similar to adhesion results, the smooth silicon sample exhibited the highest COF[25]. In contrast, the OTS-modified smooth silicon sample displayed the lowest COF. This reduction in COF can be attributed to the ordered orientation of OTS molecules when fully assembled, as depicted in Figure 4(a). This orientation leads to reduced interfacial shear strength between the tip and the surface, consequently lowering the COF. Additionally, [26]the low surface energy of the OTS SAM and diminished meniscus formation contribute to the overall reduction in friction.

Figure 3(b) also highlights that both textured surfaces (with and without OTS modification) demonstrated lower COFs compared to the smooth surface, primarily due to reduced contact area between the tip and the surface caused by texturing. However, a negligible difference in COF was observed between the two textured surfaces. This can be explained by considering the schematic in Figure 4(b). The curved nature of the textured surface induces random OTS molecule orientation, preventing the formation of the ordered structure observed on smooth surfaces. As a result, the beneficial effects of OTS orientation on reducing friction, as seen on the smooth surface, are not realized on the textured surfaces.

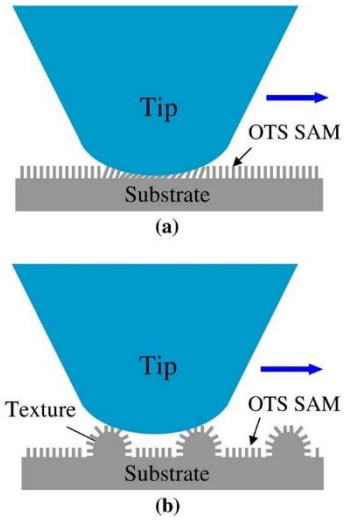

Fig. 4. Frictional behavior of tip on (a) an OTS coated smooth surface and (b) an OTS coated micro/nano-textured surface (not to scale).

3.4. Topography effect on the surface wetting properties:

To investigate the correlation between surface topography and wetting properties, four sample groups (A, B, C, D) with distinct topographies were fabricated by varying a-Si thickness and annealing conditions. Specific process parameters for each group are as follows:

Group A:100 nm a-Si, annealed at 850 °C for 5 s

Group B: 300 nm a-Si, annealed at 750 °C for 10 s

Group C: 200 nm a-Si, annealed at 800 °C for 20 s

Group D: 400 nm a-Si, annealed at 800 °C for 15 s

Figure 5 presents representative SEM micrographs of the MNTSs from each group after OTS SAM modification. Large-scale SEM images (5000x magnification) are accompanied by corresponding WCA images and higher magnification (20,000x) SEM images for detailed texture analysis.

The four samples exhibit significantly different surface topographies and texture coverage. Groups A, B, and C display surfaces covered with isolated polycrystalline silicon nano/micro-islands, forming a random nano/micro-textured structure. In contrast, Group D presents a surface network of larger silicon grains protruding from the substrate.

The WCAs of all OTS-modified textured samples exceed that of the OTS-modified smooth surface, with a maximum of 155°[4]. This enhancement in hydrophobicity aligns with the Cassie-Baxter model, which describes wetting behavior on rough surfaces. By calculating the solid surface area fraction for each sample using ImageJ and applying the Cassie-Baxter model with the known WCA of the OTS-modified smooth surface (112°), predicted WCAs of 160°, 155°, 142°, and 131° were obtained for Groups A, B, C, and D, respectively. While these predictions correlate well with experimental data for Groups B, C, and D, the Cassie-Baxter model is less applicable to Group A due to its sparse and short textures, which likely result in water droplet contact with the underlying substrate.

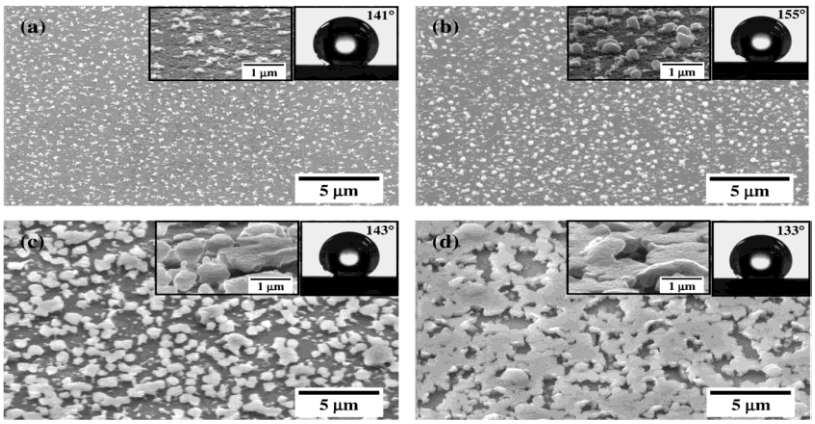

Fig. 5. SEM micrographs of four textured samples of different topographies after the OTS SAM deposition. The left insets are higher magnification SEM images of the surfaces taken at 70° tilt angle. The right insets are optical images of a water droplet on the surfaces. (a) 100 nm a-Si, 10% coverage, WCA= 141°, (b) 300 nm a-Si, 15% coverage, WCA= 155°,(c)200 nm a-Si, 34% coverage, WCA= 143°, and (d) 400 nm a-Si, 50% coverage, WCA= 133°.

3.5. Topography effect on the surface adhesion and friction properties:

Figure 6(a) reinforces the observation that OTS-modified surfaces exhibit significantly lower adhesion forces compared to smooth silicon surfaces, even when considering the difference in tip radius (100 µm vs. 5 µm). A strong correlation between adhesion performance and surface wetting properties is evident, with samples exhibiting higher WCAs demonstrating lower adhesion forces. The sample with the highest WCA displayed the optimal adhesion performance.

For indentation depths up to 50 nm, minimal adhesion force differences were observed between samples A (100 nm a-Si) and C (200 nm a-Si) due to their similar WCAs. However, at 80 nm indentation depth, sample A exhibited slightly higher adhesion forces compared to sample C. This can be attributed to the relatively smaller texture size and height of sample A, resulting in greater deformation and reduced tip-substrate distance. Samples fabricated from 400 nm a-Si (sample D) demonstrated higher adhesion forces than the other textured samples (A, B, C) due to its lower WCA and increased surface texture coverage. Among all OTS-modified samples, the smooth silicon surface exhibited the highest adhesion force.

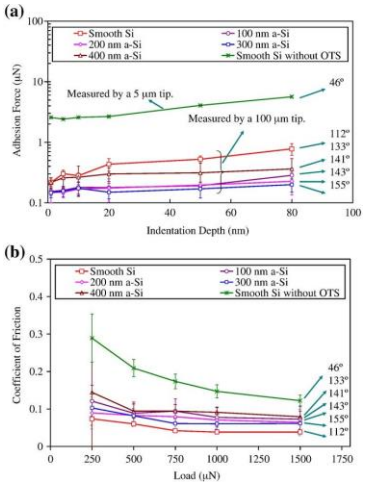

Fig. 6. Comparisons of (a) adhesion and (b) friction properties of a smooth and various micro/nano-textured samples after OTS SAM modifications.

The frictional performance of OTS-modified samples exhibited significant improvement compared to smooth silicon surfaces, as illustrated in Figure 6(b). Consistent with previous findings, the OTS-modified smooth silicon surface demonstrated the lowest coefficient of friction (COF). This behavior is attributed to the ordered orientation of OTS molecules during sliding, which reduces interfacial shear strength and consequently lowers COF. Additionally, the low surface energy of the OTS SAM and reduced meniscus formation contribute to the observed friction reduction.

For OTS-modified textured surfaces, reduced contact area due to surface texturing led to lower COFs. However, the curved nature of the textures resulted in random OTS molecule orientation, limiting the effectiveness of OTS modification in reducing friction compared to its impact on smooth surfaces.

Figure 6(b) also reveals a correlation between wetting properties and COF for the textured surfaces: higher WCAs corresponded to lower COFs. Vertical displacement measurements during sliding indicated texture deformation without removal, suggesting the ability of the textures to withstand high contact pressures.

4.Conclusions:

Hydrophobic Micro/Nano-Engineered Surfaces with Enhanced Adhesion and Friction:

This study investigated the impact of OTS SAM modification and a-Si AIC-induced micro/nano-texturing on the wetting, adhesion, and friction properties of silicon substrates. The combined application of these techniques resulted in a significant adhesion force reduction (over 90%) and the creation of superhydrophobic surfaces exhibiting a WCA of 155° and a sliding angle below 1°.

A strong correlation was observed between the adhesion and friction performance of OTS-modified textured surfaces and their wetting properties, with higher WCAs corresponding to improved adhesion and friction behavior. Furthermore, the study demonstrated that OTS modification alone can reduce the COF of a smooth silicon oxide surface by approximately 75%.

References:

[1] K. Komvopoulos, J. Adhes. Sci. Technol. 17 (2003) 477.

[2] R. Maboudian, R.T. Howe, J. Vac. Sci. Technol. B 15 (1997) 1.

[3] N. Tambe, B. Bhushan, Nanotechnol. 16 (2005) 1549.

[4] A.B.D. Cassie, S. Baxter, Trans. Faraday Soc. 40 (1944) 546.

[5] E. Martines, K. Seunarine, H. Morgan, N. Gadegaard, C.D.W. Wilkinson, M. Riehle, Nano Lett. 5 (2005) 2097.

[6] L. Feng, S. Li, Y. Li, H. Li, L. Zhang, J. Zhai, Y. Song, B. Liu, L. Jiang, D. Zhu, Adv. Mater. 14 (2002) 1857.

[7] W. Ming, D. Wu, R. van Benthem, G. de With, Nano Lett. 5 (2005) 2298.

[8] T. Sun, G. Wang, H. Liu, L. Feng, L. Jiang, D. Zhu, J. Am. Chem. Soc. 125 (2003) 14996.

[9] X. Feng, L. Feng, M. Jin, J. Zhai, L. Jiang, D. Zhu, J. Am. Chem. Soc. 126 (2004) 62.

[10] H.Y. Erbil, A.L. Demirel, Y. Avci, O. Mert, Science 299 (2003) 1377.

[11]J. Li, J. Xu, L. Fan, C.P. Wong, Proc. of the 54th Electronic Components and Technology Conf. (ECTC), Las Vegas, USA, June 1–4, 2004, vol. 1, 2004, p. 943.

[12] Y. Li, G. Shi, J. Phys. Chem. B 109 (2005) 23787.

[13] H. Liu, I. Ahmed, M. Scherge, Thin Solid Films 381 (2001) 135.

[14] J. Ding, P. Wong, J. Yang, Wear 260 (2006) 209.

[15]Y. Fu, J. Ding, J. Yang, J. Microelectromech. S. 10 (2001) 41.

[16] O. Nast, A.J. Hartmann, J. Appl. Phys. 88 (2000) 716.

[17] J. Schneider, R. Heimburger, J. Klein, M. Muske, S. Gall, W. Fuhs, Thin Solid Films 487 (2005) 107.

[18] J. Henry, J. Livingstone, Adv. Mater. 13 (2001) 1023.

[19] O. Nast, S. Brehme, S. Pritchard, A.G. Aberle, S.R. Wenham, Sol. Energy Mater. Sol. Cells 65 (2001) 385.

[20] M. Zou, L. Cai, W. Brown, Electrochem. Solid-State Lett. 8 (2005) G103.

[21] S. Gall, M. Muske, I. Sieber, O. Nast, W. Fuhs, J. Non-Cryst. Solids 299 (2002) 741.

[22] R. Premachandran Nair, M. Zou, Surf. Coat. Technol. 203 (2008) 675.

[23] Y. Song, R. Premachandran Nair, M. Zou, Y.A. Wang, Nano Research 2 (2009) 143.

[24] E. Yoon, S.H. Yang, H. Han, H. Kong, Wear 254 (2003) 974.

[25] S.A. Mirji, Surf. Interface Anal. 38 (2006) 158.

[26] B. Bhushan, H. Liu, Phys. Rev. B 63 (2001) 245412.